A new portable penetrometer for measuring the viscosity of active lava

M A Harris, S. Kolzenburg, I. Sonder, Oryaëlle Chevrel

Post-print version of the article published in Review in Scientific Instrument. Vol. 95, 065103 (2024) https://doi.org/10.1063/5.0206776

A new portable penetrometer for measuring the viscosity of active lava

M.A. Harris[1,a], S. Kolzenburg[1] , I. Sonder[1], M.O. Chevrel[1,2,3,4]

[1]*Department of Geology University at Buffalo, 126 Cooke Hall Buffalo, NY 14260-4130, USA*

[2]*Université Clermont Auvergne, CNRS, IRD, OPGC, Laboratoire Magmas et Volcans, 63000 Clermont-Ferrand, France.*

[3]*Université Paris Cité, Institut de physique du globe de Paris, CNRS, 75005 Paris, France*

[4]*Observatoire volcanologique du Piton de la Fournaise, Institut de physique du globe de Paris, 97418 La Plaine des Cafres, France*

a) Corresponding Author: martin.a.harris95@gmail.com

ABSTRACT

Viscosity is a fundamental physical property of lava that dictates style and rate of effusive transport. Studies of lava viscosity have predominantly focused on measuring re-melted rocks in the laboratory. While these measurements are well-constrained in temperature, shear rate, and oxygen fugacity, they cannot reproduce the complexities of the natural emplacement environment. Field viscosity measurements of active lava are the only way to fully capture lava's properties, but such measurements are scarce, largely due to a lack of easy-to-use, portable, and accurate measurement devices. Thus, there is a need for developing suitable field instruments to help bolster the understanding of lava. Here we present a new penetrometer capable of measuring a material's viscosity under the harsh conditions of natural lava emplacement. This device uses a stainless-steel tube with a semi-spherical tip fixed to a load cell that records axial force when pushed into a material, while simultaneously measuring the penetration depth via a free-moving tube that is pushed backward along the penetration tube. The device is portable (1.5 meters long, 5.5 kg in weight), and uses a single-board computer for data acquisition. The penetrometer has an operational range from 2.5×10^2 to 2.1×10^5 Pa s and was calibrated for viscosities ranging from 5.0×10^2 to 1.6×10^5 Pa s. It was deployed to the 2023 Litli-Hrútur eruption in Iceland. These field measurements successfully recorded the *in situ* viscosities of the lava in the range of 1.2×10^4 to 3.4×10^4 Pa s, showcasing it as an efficient method of measuring natural lava viscosity.

Post-print version of the article published in Review in Scientific Instrument. Vol. 95, 065103 (2024) https://doi.org/10.1063/5.0206776

I. INTRODUCTION

For magmas, viscosity is a fundamental physical property that greatly influences their transport and emplacement, such as ascent rates, effusion rates, and flow rates (Hon et al., 2003; Kauahikaua et al., 2003; Cashman et al., 2013). In volcanic processes, the viscosity of silicate melts can vary from ~10^1-10^{12} Pa s. This wide range in viscosity is predominantly due to variations in the composition, temperature, volume of suspended solids, and exsolved fluid or gas phases. Since lavas are three-phase mixtures containing melt, bubbles, and crystals, their bulk rheology is directly linked to the volume fraction of each phase (Pinkerton and Stevenson, 1992; Harris and Allen, 2008; Mader et al., 2013; Kolzenburg et al., 2022).

There have been numerous experimental, empirical, and analog investigations of lava rheology that study different phase proportions in the mixture. This includes single-phase melts (Shaw, 1969; Hess and Dingwell, 1996; Giordano and Dingwell, 2003; Giordano et al., 2008; Hobiger et al., 2011), two-phase (melt+crystal) mixtures (Marsh, 1981; Pinkerton and Stevenson, 1992; Sato, 2005; Chevrel et al., 2015; Moitra and Gonnermann, 2015; Kolzenburg et al., 2019), and two-phase (melt + bubble) mixtures (Llewellin et al., 2002; Rust and Manga, 2002; Truby et al., 2015). For high-viscosity rocks (felsic), several studies successfully investigated the rheological properties with three phases (melt+liquid+gas) (Hess et al., 2007; Avard and Whittington, 2012; Pistone et al., 2013; Heap et al., 2014; Dobson et al., 2020). However, due to the time it takes to conduct experimental measurements on melted low-viscosity rocks (mafic) at atmospheric pressure in the laboratory, all the volatiles are released. Thus, currently, the only method capable of measuring natural three-phase mafic lava viscosities is to perform in situ measurements on active flows (e.g., Chevrel et al., 2018a, 2019, 2023).

To measure high-temperature lava properties on active volcanoes, it is essential to have instruments that can withstand the temperatures present in natural lava flows, are portable, and acquire data swiftly and accurately. These considerations have guided the development of the instrument presented here. This new lava penetrometer has undergone comprehensive testing in the laboratory and has gone beyond a proof-of-concept with its use at an active volcanic eruption in Iceland, and shows durability and accurate results across a range of viscosities from 10^2 to 10^5 Pa s. Here, we present in detail the background, procedure, and capacity of this novel instrument for measuring natural high-temperature lava viscosities.

II. BACKGROUND

2.1 Field Viscometry of Lava

Approaching active lava and conducting measurements requires bespoke instruments that can withstand extreme conditions and yield accurate data. As a result, there are only twelve published attempts at measuring active lava rheology (Einarsson, 1949, 1966; Shaw et al., 1968; Gauthier, 1973; Pinkerton and Sparks, 1978; Panov et al., 1988; Keszthelyi, 1994; Pinkerton et al., 1995b, 1995a; Pinkerton and Norton, 1995; Belousov and Belousova, 2018; Chevrel et al., 2018a, 2019).

Direct measurements of lava viscosity date back to 1949 (Einarsson, 1949). Early field studies used crude instruments such as metal rods pushed into lava using body weight, while later studies used motor-driven devices with electronic data acquisition systems. Prior work on field viscometers shows that the results can be extremely useful in characterizing complex natural lava rheology. For a more elaborate review see Chevrel et al., (2019) and the references therein.

Two categories of devices have proven useful in field rheology. Firstly, a penetration type, that records the force needed to push a defined geometric shape into the lava. Secondly, a rotational viscometer that records the torque and rotational speed of a shear vane immersed in the lava (Chevrel et al., 2019). There are advantages and disadvantages to both methods, but overall, the rotational viscometers are effective at low-viscosity ranges (~10^2-10^4 Pa s) whereas the prior penetrometers have been used in higher viscosity materials (~10^3-10^6 Pa s). Recent advances in rotational field viscometers are detailed in Chevrel et al., (2023).

2.2 Penetrometers

Penetrometers are scientific and industrial tools that have broad applications. The overall concept of all penetrometers is to push a fixed geometric shape into a desired medium and record the amount of force exerted to penetrate at a given rate or to a defined depth. The shapes of the penetration head range from rounded, squared (or flat), conical, concave, and even mesh-webbing. Within soil science, hand-held penetrometers are commonly conically tipped and used to assess soil strength properties, often as a measure of Impulse (a change in momentum as Force × time) which in turn have implications for water content, soil density, drainage capacity, and root growth availability (Herrick and Jones, 2002; De Moraes et al., 2014; Kirkham, 2014). The agricultural

penetrometers can be manually operated as static drivers pushed by an operator into the soil, or driven with hydraulic pressure, and readouts are made with a loadcell and/or strain gauge. Other approaches include dynamic methods that use the kinetic energy of known, freefalling masses to drive a penetrating device into the soil (Herrick and Jones, 2002). Dynamic cone penetrometers are also widely used in road and infrastructure engineering, where the strength of pavement is relevant to road construction and maintenance (Boutet et al., 2011). Likewise, concrete condition-assessing penetrometers are used to monitor the degradation of sewer systems that may need restoration (Hall et al., 2022). Additionally, portable penetrometers are also developed by snow scientists that investigate the strength of snowpack layers (Schneebeli and Johnson, 1998; Floyer and Jamieson, 2010). Often these snow penetrometers are capable of measuring depths up to 1.5 m and are controlled via step-motors or manually guided through a platform into a snow layer of interest. Lastly, industrial penetrometers are used for food quality control for rheological consistency or overall material strength (Tanaka et al., 1971, 1972; Dubbelboer et al., 2018; Jantra et al., 2018).

While many penetrometers already exist to measure a material's properties in the field, they do not meet several criteria for *in-situ* measurements of lava (*i.e.,* a molten rock at a temperature above 1000°C). The materials for such instruments need to be constructed out of high-temperature resistive metals (*e.g.,* stainless steel). A lava penetrometer needs to be long enough to safely reach and penetrate lava without the operator getting exposed to excessive heat (*i.e.,* 1.5-2 m). Portability is also essential, as active lava environments are dynamic and volcanoes are hard to predict. Thus, a lava penetrometer must be light so that it can be carried and moved swiftly by one person if needed. The measurement procedure must also be efficient to limit exposure to high temperatures, reduced oxygen conditions, noxious/acid gases, and dusty environments. Therefore, self-contained electronic sensors are preferred and the use of external apparatus to set up the measurements like a stand, tripod, or fixed rig is suboptimal. Lastly, while many other penetrometers focus on the force-derived strength of compressible solids (*i.e.,* soil), for lava investigations we seek the viscosity (*i.e.,* strain–rate–stress relationship) of an incompressible liquid. Thus, simultaneous acquisition of force and displacement rate is needed (see discussion below). These criteria have led some past volcanologists to design lava penetrometers for field use (Einarsson, 1949; Pinkerton and Sparks, 1978; Panov et al., 1988; Belousov and Belousova, 2018,

Gauthier 1973). A summary of the three main types of lava penetrometers used in field studies is presented below.

2.2.1 Mechanics of Existing Field Penetrometers for Lava Viscometry

1) A simple rod with a semi-spherical head is inserted into lava, and viscosity is estimated from the force used to insert at a given rate (Einarsson, 1949; Pinkerton and Sparks, 1978; Panov et al., 1988; Belousov and Belousova, 2018). This method relies on the assumption that the potential effect of lava sticking to the rod is negligible and thus calculates viscous drag based on Stokes' Law (*i.e.*, falling sphere viscometry).

2) A "ballistic" spear is shot at high (presumed constant) speed into lava. The viscosity is determined via calibration of the depth of penetration in known standard liquids. Gauthier (1973) employed this method on lavas from Mount Etna in 1971, to overcome limitations that simple penetrometers experience as the lava cools around it during slow penetration. However, this method encounters major limitations as it penetrates the outer crust before reaching the interior lava. The distance of penetration depends on the combined resistance forces caused by the outer crust and interior lavas. The result is an average viscosity measurement over the viscosity gradient from the outer, cooler, almost solid crust to the hot, molten liquid (Gauthier, 1973). Also, the path of the arrow before penetration varies every time so the kinetic energy available for penetration varies, making the standard liquid calibration unprecise. Finally, it is unclear whether the strain rates induced in the crust allow the lava to remain in the viscous relaxation field or whether it pushes it into the elastic regime (Alidibirov and Dingwell, 1996).

3) An encased spring-loaded, piston-driven device, deployed by Pinkerton and Sparks (1978) on Etnean lavas. The device is preheated and inserted through the crust before the piston is activated, thereby overcoming the crust-forming limitations of the prior two device types. However, the use of a piston device still encounters issues as the spring does not fully expand all the way each time, which yields inconsistencies in the measurements (Pinkerton, 1978). Additionally, the casing for the piston introduces a large volume of metal within the lava, thus increasing the likelihood of large-scale quenching around the inserted device and thereby influencing the rheological properties in the localized sampling area. Furthermore, the force is dictated by the spring and thus the range of accessible viscosities is predetermined and low. Lastly,

the maximum possible piston penetration is ~9 cm, thus limiting the measurement within that restricted depth (Pinkerton, 1978).

To summarize, prior penetration-type devices have employed various techniques that aim to inform on the rheological properties of natural lava. However, some methods have resulted in only qualitative data that is difficult to pair with higher precision results obtained from rheological studies in the laboratory (*e.g.,* Einarsson, 1949; Gauthier, 1973), and others were not suitable (or calibrated) for a wide range of lava viscosities (e.g., Pinkerton and Sparks, 1978; Panov et al., 1988; Belousov and Belousova, 2018). Also, none of the prior devices can precisely characterize lava crust thickness because their force and displacement determinations have remained decoupled, posing a limitation on measuring the full viscous gradient of cooling lava. Finally, the combination of field rheology and textural characterization that is required to tie rheological parameters to the textural state of the multiphase suspension are absent for field-penetrometer measurements.

The presented penetrometer instrument aims to fill these gaps with a particular focus on:

1. Optimization of the instrument's design and sensors to work best for the expected (apparent) viscosity range for mafic lavas (*i.e.,* 10^2-10^5 Pa s during *in-situ* viscosity measurements at active lava flows). This requires simultaneous recording of force and displacement during penetration.
2. Improvement of the ease of operation and mobility so that such a device can be easily deployed in the field with a high success rate of accurate lava viscosity measurement.
3. The use of standard mechanical and electronic parts and sensors which are available in large enough numbers, so that costs can be lowered and individually replaced with an alternative if necessary.
4. Extensive testing and calibration of each instrument variant (penetrator geometry), such that results can be compared with datasets generated in high-temperature rotational viscometry-based lab-scale measurements which typically work with re-melted material.
5. Open availability of all parts and plans of the instrument's design and data acquisition code.

III. INSTRUMENT DESCRIPTION

The goal of our penetrometer device is to measure the force needed to penetrate a viscous lava at a given rate (distance over time). To measure penetration force, we mount a force gauge between a base element made of aluminum and a long tube made of stainless steel, the 'penetration tube' (19 mm diameter, 1.65 mm wall thickness, 150 cm long) (Fig. 1A). The penetration tip, a stainless-steel hemisphere (38.1 mm diameter) is mounted to the end of this tube. In theory, other tip geometric shapes and sizes could be used but would require a separate set of calibrations (see section below). The penetration tube was chosen over a rod to reduce the device's weight but retain rigidity, and the tube also allows the steel tip to be slotted within or exchanged if it becomes damaged. This tip is tapered with rounded edges on the back side (opposite to the direction of penetration) to aid the extraction process when the measurement is complete. The overall diameter of the tip is greater than that of the penetration tube, thus eliminating the effect of friction of lava as the penetration tube moves into the medium. Linear bearings restrict the possible motion of the penetration tube to the force sensor's relevant axis and fix it to the base element (Fig. 1B). The linear bearings for the penetration tube were selected to optimize stability, not for maximum travel speed. We use commercial hand-held size force gauges with three interchangeable options: capable of reading forces up to 1000, 500, and 100 Newtons (N), respectively. The reported accuracy for each gauge was ±2.0 N, ±1.0 N, and ±0.2 N, respectively. The desired gauge is selected based on the expected viscosity range that is encountered in the field to facilitate the most sensitive and accurate measurement. The force gauge is wired to a Raspberry Pi (or equivalent single-board computer (SBC)) through a USB serial port.

To measure displacement, a lightweight tube, the 'displacement tube', is mounted onto the penetration tube, also using linear bearings (Fig. 1A). These bearings were selected to support high travel speeds at low friction. Testing showed that for the targeted viscosity ranges these friction forces are negligible to the acting penetration force. A reflecting metal disc is mounted to the displacement tube (with a slotted bottom to fit around the diameter of the penetration tube) and acts as a target for the laser time of flight distance sensor, which is fixed to the base element (Fig. 1B). As the penetration tube is pushed into the lava, the displacement tube, free-floating in the low friction bearings, and capped with a flat steel washer (for increased surface area to avoid penetration into the lava) is simultaneously displaced backward to the penetration depth. This motion brings the reflective target towards the distance sensor that registers displacement within the range of 50-400 (±5) mm and is connected to the SBC via inter-integrated circuit (I2C) pins.

Both force and displacement sensors are read simultaneously every 100 ms. The raw data is converted to Unicode (UTF-8) and SI units for Force (N) and displacement (mm) and then written to permanent storage (SD card) of the SBC in a CSV-like (comma-separated values) format. The program uses the SBC's real-time clock to control the main data acquisition loop. Sensor check and acquisition control is realized with robust flip switches which can be handled in a rough environment (see Supplementary Material (S)1 for details).

The force gauge, electrical box, penetration tube, and displacement tube all rest on a stabilizing slotted extruded aluminum profile (Fig. 1B). The mass of the penetration tube exerts a constant force on the force gauge, which depends on the angle to the vertical axis (zero in horizontal, maximal in vertical position). Therefore, the force gauge can be tarred quickly at any angle, and measurements do not need to be done only horizontally or vertically. It does, however, require the operator in the field to maintain that angle. Random deviations from the angle, for example, in rough field environments manifest themselves as analog noise in the force signal. Below described field tests show, however, that this is a manageable problem.

Handles are attached within the slots of the stabilizing bar and adjusted to positions that are comfortable for the operator's arm's length. We find that fixing one handle pointing down from the stabilizing bar and one pointing out on the side offers optimal control and ease of use, yet the choice can be made by each individual.

At 150 cm the penetrometer is a relatively long hand-operated instrument. To ease transport, it can be disassembled into smaller pieces. Along the final third of the penetrometer tube and displacement tube (region closest to the penetrometer tip), we have engineered quick-release junctions held with steel cotter pins (Fig. 1B). The disassembly also has an aspect related to safety: Though lava flows may not be the fastest known phenomenon of volcanic eruptions, the processes involved are not controllable in any way by humans and the flow progress is still hard to predict. It could therefore become necessary to leave the measurement location quickly. If the penetrometer gets stuck in cooling lava that would mean having to decide in seconds whether or not to leave the whole instrument. The ability to sacrifice only part of the instrument by quickly removing it supports safe decision making in the field.

The entire suite of electronic sensors is powered with a portable power bank fixed to an electrical box. Supplement (S)1 contains the full list of electronic parts and detailed custom-machined parts can be found on the online repository (see link below).

The rough application environment and measurement durations of 2 to 15 seconds make a fragile graphical computer screen-like display the wrong choice for this instrument. Instead, we chose to install a bright LED based 4-Digit 7-Segment display, which informs the user with pre-defined messages about the current state, and potentially not working sensors. This choice reduces the SBC's power consumption and increases the battery life (see S1 for more details). It also means that any data visualization, even for quality check only, must be done in a postprocessing step. We created a set of Python scripts that help to quickly visualize and run a standardized analysis on raw sensor records (see below). These are available together with the penetrometer software code at https://github.com/LAVAPUBMH/Lava_Field_Penetrometer.

IV. DATA PROCESSING AND CALIBRATION

Both sets of programs, for data acquisition and data analysis (see online repository for most current versions), were written in the Python scripting language because the resulting code is relatively easy to understand for most users (*e.g.,* students, researchers, and scientists who are not computer scientists) while it also runs on the somewhat less performant hardware of an SBC. Both programs use the numpy library (Harris et al., 2020); the data acquisition program further depends on several smaller libraries that enable communication with the sensors; the data analysis program uses Matplotlib (Hunter, 2007) for data visualization and user interaction. All the dependencies are published under open-source licenses.

We have created a data processing procedure with Python codes that allow standard data analysis, (*i.e.,* retrieval of speed and force as well as the viscosity, for a person without programming knowledge). Raw signals are plotted against time in a graphical user interface (GUI). The relevant time window can then be selected using the pointer/mouse, which is realized with Matplotlib's `SpanSelector` object. The relevant time window for viscosity measurement is a plateau of stable (i.e. constant or flat) force and negative, constant displacement slope (Fig. 2A). The SpanSelector can be used as many times as necessary to extract the desired data (Fig. 2B). Ultimately, once the user is satisfied with the specific portion of the penetrometer run selection, the code calculates the mean or moving-averaged (depending on user preference) force

(N) and displacement rate (m/s) (*e.g.,* Fig. 2C), which in turn can be used to calculate the viscosity using Eq.1 or Eq. 2 (See below discussion). The viscosity can also be processed with a moving average or left as raw calibrated values. Depending on the material that is measured, the operator may wish to smooth the viscosity signal or not. Both options are available in the processing code. Ultimately, the user can specify in the code what size window is desired to run the smoothing moving average function. All these codes are available at https://github.com/LAVAPUBMH/Lava_Field_Penetrometer.

The current penetrometer has undergone calibration and testing in three analog materials. One Newtonian viscosity standard oil, Cannon N190000, and two non-Newtonian materials, Tryptone (a casein-derived protein gel) and SillyPutty™. First, we measured all three materials with an Anton Paar concentric cylinder rheometer calibrated with Cannon Oils certified (#1262.01) by the National Institute of Standards and Technology (NIST). The concentric cylinder rheometer is equipped with a water bath casing that allows for temperature-controlled viscosity measurements between 2 and 60 °C. The volume of the analog material in the concentric cylinder was approximately 30 ml in each case. We developed temperature-dependent viscosity models for each of the three materials from the concentric cylinder data conducted at constant temperatures and used these models to interpolate target viscosities for the penetrometer calibration (Fig. 3 and S2). For this, we use a Vogel-Fulcher-Tammann (VFT) (Vogel, 1921; Fulcher, 1925) equation (*i.e.,* $\eta = \eta_0 \exp(-B/(T-T_0))$ to describe best the temperature dependence of the measured internal standards. A fit of the models to measured viscosities yielded correlation coefficients, $R^2 = 0.999$, 0.999, and 0.997 for N190000, Tryptone, and SillyPutty™, respectively (see S2). Calibration measurements were conducted at shear rates where non-Newtonian behavior was negligible (*i.e.,* no shear thinning, or other such effects detected). For N190000 the shear rate range was 0.555-6.940 s^{-1}, for Tryptone 0.027-0.055 s^{-1}, and for SillyPutty™ 0.014-0.033 s^{-1}.

We then conducted measurements using our penetrometer for each of the three analog materials across a temperature range of ~12-45 ˚C. The temperatures were controlled with a heating and cooling system plumbed into a 20 L water bath. Within the water bath, we placed the respective analog materials (~1.5 L of N190000, ~6 L of Tryptone, and ~8 L of SillyPutty™) in glass beakers. Tryptone and Sillyputty were measured in 10L beakers with diameters of 225 mm, and the

N190000 oil was measured in a 2L beaker with a diameter of 130 mm. The penetrometer tip is 38.1 mm in diameter. The effects of a finite container size can be neglected if the beaker radius to sphere radius > 5 (Macosko, 1994). For tryptone and Sillyputty, the relationship of the beaker to the ball radius is 112/19=5.9. For N190000, the ratio is less than 5 (67.5/19=3.6), however, our recovered viscosity values are within acceptable uncertainty to the known values of the standard oil (see below discussion and Fig. 3). We hence deem any wall effect quite negligible. Before each measurement, we ensured the material had reached thermal equilibrium with the water bath by probing the material with a PT100 thermoprobe (±0.5°C).

In the studies of Panov et al., (1988) and Belousov and Belousova (2018), assumptions were made based on the hemispherical tip of the penetrometer to use a modified version of Stokes' Law (Eq. 1) for viscosity derivation as:

$$\eta = \frac{F}{3\pi v \mathrm{R}_{eff}} \quad \text{Eq. 1}$$

where η is viscosity, F is the force of penetration, v is the speed of penetration, and R_{eff} is the effective radius of the rod. In past studies, force is typically recorded by a hand gauge, and velocity is measured by recording the time needed for penetration of the rod to a given depth (using video analysis or stopwatches), or simply timing the immersion between marked intervals on the rod manually (Panov, V.K et al., 1988; Belousov and Belousova, 2018). Although both Panov et al., (1988) and Belousov and Belousova (2018) recovered rheological values in the expected range of basaltic lava, their data reduction approach (Eq. 1) was purely based on assumptions that a hemisphere could be dealt with by halving a factor related to sphere size in the viscous drag formula (*i.e.,* 3π) and was not tested for validity with analog materials or calibration of any sort. We initially processed all the penetrometer data using Eq. 1. However, the results from all three analog materials had poor fits with the known viscosity values of our reference materials (Fig. 3). We then applied the unmodified Stokes' Law (Eq. 2) and recovered a better fit to the model curve (Fig. 3):

$$\eta = \frac{F}{6\pi v \mathrm{R}_{eff}} \quad \text{Eq. 2}$$

Yet, Stokes' Law (Eq. 2) also results in an inaccurate determination of the measured material's viscosity, as there was still a significant deviation from the known viscosities, particularly the

N190000 (124 ± 32% Pa s) and SillyPutty™ (14 ± 7% Pa s) (Fig. 3). This is likely since the penetrating geometry is a hemisphere and not a full sphere and thus, any drag effects on the back side of the sphere are that the Stokes' Law treatment relies on are absent.

We then looked to an alternative calibration procedure that modifies Stokes' Law in lieu of an empirical, force-to-penetration speed ratio (Ns/m) relationship to known viscosity. This method replaces the theoretically derived geometric constraints from a falling sphere and instead uses the signals of the force gauge and distance sensor and compares them with the viscosities of calibration materials measured in a standard concentric cylinder setup. Our results show that the force-to-displacement rate ratios (F/v) obtained with the penetrometer from the three calibration materials have linear relationships to the known viscosities of the respective materials. Thus, for the calibration, the basic assumption of a linear dependency between η and F/v is formulated

$$\eta = \frac{F}{v} m + b \quad , \qquad \text{Eq. 3}$$

where slope m replaces the fixed geometry factor $1/6\pi R$ in Equations and 2, and offset b compensates an instrument threshold. The calibration was then done by fitting Eq. 3 to measured F/v values and reporting parameters m and b (Table 1). We do not apply any correction for buoyancy forces in this procedure as the expected maximum effect lies around 0.14 N for the lighter calibration oil (N190000) and 0.42 N for non-porous, molten lava (see S3). These values are well below the sensitivities of the deployed force gauges of 1-3 N.

We choose to employ linear regressions with an offset from the origin, b in Eq. 3, as they yield the best fit with the lowest deviation from the known viscosities. The offset is not caused by the calibration material behavior or the geometrical setup (liquid's container size or penetration head diameter). It is likely caused by the penetration rod linear bearings (low friction), which stabilize the relatively long instrument assembly. Results show that calibration turned out to be best when divided into two ranges separated by a force-to-rate ratio threshold $F/v = 2\times10^3$ Ns/m (Table 1). All values above this threshold (as obtained for Trypton and SillyPutty™) are treated as *high* F/v. Values equal to or below the threshold are treated as *low* F/v (obtained from N1900000). Calibration shows that the instrument is validated only for $F/v > 500$ Ns/m and values below this point are below the current instrument sensitivity.

Furthermore, the measured signals of force and displacement contain random noise, and thus, the calculated viscosities, as given by Equation 3, are sensitive to such noise. To address this factor, we smooth the data with a moving average function that does not touch the time base. For a series of discrete values A_i measured at evenly timed times, t_i, the average is:

$$\bar{A}_i = \frac{1}{2N+1} \sum_{k=i-N}^{i+N} A_k \qquad \text{Eq. 4}$$

Here A can be penetration force, displacement, or calibrated viscosity and N is an integer that determines the size of the averaging window, $2N + 1$. The averaging window must have an odd sample number so that it is centered around the index i. Moving averages (Eq. 4) were computed for the force and displacement signals. Velocity, v, was computed as the negative time derivative of the averaged distance, $\bar{D}$: $v = -d\bar{D}/dt$ (see S4 for details). The time derivative was approximated with the central difference scheme. The negative derivative is necessary because the distance (from the displacement sensor) decreases at a positive speed during measurement.

Overall, calibrated values lead to smaller deviations than the Stoke's Law method (Fig. 3). We find that the calibrated results of the N190000 oil viscosity range have a mean deviation from the known viscosity of 9 ± 6% (number of measurements, n =10). The calibrated results of the Tryptone and SillyPutty™ viscosity range have a mean deviation from the known viscosity of 4 ± 4% (n=19) and 7 ± 3% (n=10), respectively

Table 1: Calibration constants for the two F/v ranges

	***F/v* (Ns/m)**	***m* (1/m)**	***b* (Pa s)**
low	$\leq 2\times10^3$	2.5	-1112
high	$> 2\times10^3$	3.1	-1687

The penetrometer, when calibrated as outlined above, can accurately measure the viscosities of materials from 5.0×10^2 to 1.6×10^5 Pa s (Fig. 4). A catalog of our measured, known, and calibrated viscosities for the three analog materials can be found in S2. To accurately use Eq. 3 to determine viscosity with this penetrometer, it is essential for each different force gauge or distance sensor to undergo this calibration procedure.

Post-print version of the article published in Review in Scientific Instrument. Vol. 95, 065103 (2024) https://doi.org/10.1063/5.0206776

V. MEASUREMENTS OF ACTIVE LAVA: ICELAND 2023

The field instrument we present here is made for *in-situ* rheological characterization of high-temperature material: *i.e.*, active lava flows. To assess the effectiveness of the newly developed penetrometer device, we tested it at an active volcanic eruption. For this, we performed measurements on a slowly moving ‘A‘ā lava front of the Litli-Hrútur 2023 eruption on the Reykjanes Peninsula in Iceland (Fig. 5).

For field measurement, the ideal configuration involved two scientists: One carried and operated the field viscometer and the other assisted in watching out with a water bucket for quenching the lava if needed. Before any measurement we rested the penetrometer tip near the incandescent lava to pre-heat the metal to avoid lava quenching on the instrument (Fig. 5C). In a natural context, when the molten lava is exposed to the air, it forms a cooler outer crust. ‘A‘ā lavas are blocky masses that periodically collapse and break apart as they advance over time. The access to interior molten melt was not always successful, and some measurements encountered impermeable crust or bumped into obscured fragments of crust within the interior of the lava. Therefore, we repeated measurements across a small section of exposed lava (30 cm window, Fig. 5C) to assess the reproducibility of the potentially heterogeneous lava. This type of dynamic measurement technique that acquires force and displacement simultaneously within a heterogeneous lava area is only possible with the device presented here.

To start the measurement, we would focus on areas that had molten material available and where the displacement tube could rest on an outer portion of the cooled crust (Fig. 6A). When needed, we removed the cooler crust using a hammer or metal pole, so we could directly access the molten interior. The operator would steadily push the penetrometer into the lava for ~20 cm depth, over ~2 to 15 seconds (*e.g.,* Fig 6B and C). Once the maximum displacement was reached, the penetrometer was extracted from the lava, typically leaving a hole the diameter of the stainless-steel tip for a matter of seconds (*e.g.,* Fig 6D). If any lava had stuck to the penetrometer during extraction, it would be collected from the quench bucket and cataloged as field samples linked to the specific measurement. Additionally, thermal readings were conducted just after the viscosity measurements at the same site using K-type thermocouples (±1˚C). The quenched lava samples were cataloged and brought back for textural and chemical analyses (see S5) and for further geological studies. Despite the extreme conditions of temperatures up to ~1200˚C and corrosive

gases (*e.g.,* H_2S), there was no degradation of any mechanical parts of the penetrometer, including the repeatedly immersed penetrometer tube and tip.

Natural lava is much more heterogeneous than analog materials and prepared, re-melted field samples used in the laboratory. Erupting lava often has viscosity gradients caused by crust formation, temperature gradients, or channelized flow fields. These changes in viscosity can be measured with the penetrometer in a single run if such changes are continuous and relatively slow, such that the steady-state assumption of Stoke's law is approximately satisfied. Slow in this context means that the change of viscosity causes either a change of measured force or penetration speed. None of these changes must be caused by a 'sudden' change in the driving force (here the operator). Furthermore, the viscosity gradient cannot be large enough to cause changes in inertial forces around the penetrometer head. Overall, these conditions are typically satisfied if both measured displacement and force profiles are smooth without major bumps.

In total, we performed nine penetrometer measurements within the 15 m wide and 3 m tall lava front, and the results are shown in Figure 7. Runs 1-2 were done back-to-back, followed by a break of ~30 minutes before runs 3-5 were conducted. Runs 6 to 9 were done 25 minutes later, and just after a large block collapsed from the 'A'ā pile exposing a ~1.5 m window of molten interior. The overall range of viscosities recovered from the measurements spanned 1.2×10^4 to 11.0×10^4 Pa s, with penetration depths between ~0.14 and 0.15 m (Fig. 7A). The viscosities shown with depth (Fig. 7A) were processed with a moving average (Eq.4) window of nine. We observe in runs 2 to 4 heterogeneous viscosities with depth, with initially high and/or fluctuating viscosities, followed by a rapid decrease and an eventual flattening of values towards the deeper parts of the measurements. We interpret this as penetration through varying thicknesses of cooler crust and eventually reaching the molten interior indicated by the latter stable viscosity readings. In contrast, the viscosities from the other measurements do not record penetration of highly variable crust (*e.g.,* lava was freshly exposed after a block collapsed), and instead remain stable across the penetration (Fig. 7A). This highlights the ability of this new device to accurately characterize spatial variations in viscosity over the penetration distance – a capability that no previous instrument that was used on active lavas had. The temperatures of the molten interior revealed that the earlier and later runs (Runs 1-2, Runs 6-9) had slightly higher temperatures than the middle runs (Runs 3-5).

We investigated the temperature-specific viscosity of each run by only processing the stable viscosity regions from Figure 7A, as these are the areas that best represent the molten interior. We find that the viscosity for the Iceland lavas at this location ranges from 1.2×10^4 Pa s at 1152°C, to 1.8×10^4 Pa s at 1150°C, and to 3.4×10^4 Pa s at 1148°C (Fig. 7B). Overall, the ranges of the ʻAʻā lava measured with the penetrometer are within the expected magnitudes of basaltic ʻAʻā lava (Hon et al., 2003; Robert et al., 2014; Sehlke et al., 2014). The field tests highlight that the device recovers accurate viscosity data and can track relatively small changes in viscosity over a narrow temperature range at high temporal and spatial resolution.

VI. DISCUSSION

A. Advantages and limitations of the instrument

The penetrometer device has the potential to measure a viscosity range of ~2.5×10^2 to 2.1×10^5 Pa s based on plausible field measurement constraints from the 10-500N force over measurement timescales of 2-30s. We view anything outside this range as either being too small in measurement duration for accurate processing or beyond the physical limits of most adult operators. We have specifically calibrated the device to viscosity ranges from 5.0×10^2 to 1.6×10^5 Pa s. The stainless-steel penetration tube, displacement tube, and tips are capable of withstanding temperatures up to 1200℃ for moderate timescales (*i.e.,* minutes). The high-temperature performance is highlighted by the successful use in volcanic settings, where no lava-submersed parts of the penetrometer broke, bent, or were damaged over two weeks of field measurements. The quick releases at the far end of the device (see Fig. 1) ensure that even if parts exposed to high temperatures were to incur damage, they can quickly be exchanged with replacement parts without needing to rebuild the entire device.

Additionally, the size (1.5 m length), and weight (~5.5 kg) of the penetrometer allow for operation by a single person with ease, making it highly mobile. Furthermore, this new penetrometer has self-contained electronic data acquisition for simultaneous force and displacement rates during measurements, a characteristic that is novel in comparison to all other penetrometers used for field lava rheology. All operations are done using only two switches, which are designed to be easily operated single-handedly by the device operator even with thick gloves. Lastly, the material costs of this penetrometer are quite low (see S1), making it an attainable instrument for most research centers around the world.

In earlier versions of the prototype, we had a K-type thermocouple fed through the tip of the penetrometer. However, extensive laboratory and field tests at high temperatures revealed that the duration of penetrometer measurement is too short for a thermocouple to equilibrate with its surroundings. Thus, we removed the thermocouple in the current device so that all the data acquired yield high confidence. Since temperature information is an important component of lava rheology, we suggest that separate temperature readings are done with a device that can withstand long immersion timescales in material adjacent to where the penetrometer measurements are completed. For our case, we used standard stainless-steel sheathed type K thermocouples.

Additionally, in contrast with a field rotational viscometer that increases and decreases rotational speeds (Chevrel et al. 2023), the penetrometer presented here has no defined way of varying the imposed strain rate throughout an individual measurement. This poses a limitation as not all materials have linear stress-strain relations (*e.g.,* Bingham, Herschel Bulkley, *etc.*) like natural lavas (Kolzenburg et al., 2022). To probe varying strain rates, the operator can attempt to manually vary the force at which the penetrometer is pushed into the material on subsequent measurements. However, in the application of volcanology, this systematic repetition may not always be feasible in dynamic lava flow settings as sometimes only one measurement is possible in one location.

Lastly, the current device has a limitation of measurement calibration for viscosities lower than ~500 Pa s. It is possible that employing different force gauges with greater sensitivity to compressive strain may yield better results at these lower viscosity ranges, but further testing would be required to verify that approach. Alternatively, the combination with a rotational viscometer able to measure viscosity within (10 to 650 Pa s; Chevrel et al. 2023) is suggested to describe the full viscosity range for natural lavas.

B. Effectiveness for field lava rheology and other geomaterials

The typical range of mafic eruption viscosities lies within 10^1-10^5 Pa s (Harris and Rowland, 2015 and references therein). Thus, the capable range for this penetrometer (10^2-10^5 Pa s) fits well within the expected natural range of lava. Additionally, this penetrometer overlaps the upper end of the viscosity capabilities for a field rotational viscometer, (10-10^4 Pa s) (Chevrel et al., 2019). This means that in some settings, the penetrometer can be used in conjunction with, or, in place of a field rotation viscometer to obtain rheological values of lava flows. In other instances,

particularly when the viscosity is intermediate to high in mafic lavas (*i.e.,* $\geq 10^4$ Pa s), like in the presented field measurements, the penetrometer is currently the only instrument capable of obtaining accurate *in-situ* rheological data. These characteristics support the concept of this penetrometer's applicability for *in-situ* work on lava flows, and the successful deployment of this device during the Iceland 2023 eruption at Litli-Hrútur served to validate the instrument's capabilities.

The investigation of lava rheology through field measurements stands alone as the only current method to investigate the properties of natural high-temperature lava. As lava cools, it degasses and crystalizes until eventually, it reaches a rheological threshold where it is unable to flow (Kolzenburg et al., 2019, 2020; Di Fiore et al., 2021). Currently, numerical lava-flow models implement lava viscosities yet they lack field-validated values (*e.g.,* Chevrel et al., 2018b). The capabilities of this new penetrometer, including portability and durability allow for accurate *in-situ* measurements across various locations at the same lava flow. This raw field data can be used to discern the rheological evolution of an effusive eruption, and thus be implemented into future models that can benchmark their predictions off natural lava viscosity data. This type of work not only contributes to the field of lava rheology but also has the potential to aid populations that live in and around active volcanic regions and rely on rapid eruptive forecasting for their safety.

While the primary objective of this penetrometer device is to obtain viscosities of high-temperature lavas in the field, we highlight that there are other potential applications for this instrument, which may include modifying the force sensor sensitivity to match a desired viscous range. Other geomaterials such as mudflows, debris flow avalanches, and snowpacks are investigated for their rheological properties with penetrometers much like lava flows, to better understand the risk of speed and runout distances during these hazardous events (Schneebeli and Johnson, 1998; Floyer and Jamieson, 2010; Widjaja, 2019). Many of these geohazards studies rely on modeling or experimental data (e.g., Rognon et al., 2008; Huang and Aode, 2009; Kostynick et al., 2022) and the use of our new field penetrometer on these complex heterogenous geomaterials has the potential to benchmark the models and experiments to natural data obtained in the field.

VII. CONCLUSION

We present a new penetrometer device that can withstand extreme conditions such as volcanic environments including high temperatures (tested to ~1150˚C) and corrosive gases. The

device is engineered with stainless steel and has self-contained electronics, all powered by a small portable power bank. The device is portable and can be operated by a single person, with a length of ~1.5 m and a weight of ~5.5 kg. To our knowledge, this device is the first of its kind to have high-temperature resistivity, simultaneous force and displacement data acquisition, and a calibrated range of data acquisition from 10^2-10^5 Pa s. The penetrometer's durability and effective measurement range make it ideal for *in-situ* lava viscosity studies. We demonstrate that this penetrometer is effective for field measurements through its use during the 2023 Litli-Hrútur eruption in Iceland. Here, the penetrometer recorded the *in-situ* rheology of lavas from 1.2×10^4 to 3.4×10^4 (Pa s) viscosities at temperatures from 1148-1152˚C. The continued use of this instrument at future eruptions will provide the necessary data that is currently lacking to better understand the rheology of natural multiphase lava.

VIII. SUPPLEMENTARY MATERIAL

Three supplementary materials (S) accompany this manuscript.

S1: Penetrometer Parts and Data Acquisition Process

S2: Analog Material Viscosities, Measured, Known, and Calibrated

S3: Buoyancy Effects

S4: Example of Moving Averages of Penetration within Heterogenous Lava

S5: Geochemistry of Iceland Lava

IX. AUTHOR CONTRIBUTIONS

M.A. Harris and S. Kolzenburg conceptualized the apparatus design, geometry, and measurement principle. Additionally, M.A. Harris created the data acquisition chain, engineered the electronics and software, performed tests and calibrations, and led the formation of the article. I. Sonder assisted with data acquisition development and data analysis. M.O. Chevrel and M.A. Harris conducted field measurements in Iceland. S. Kolzenburg and M.O. Chevrel supervised and guided interpretations of the instrument rheological data. All authors contributed to the writing of the article.

X. ACKNOWLEDGMENTS

We thank Dr. Thorvaldur Thordarson, Dr. Ármann Höskuldsson, Dr. William Mooreland, and Méline Payet—Clerc of the University of Iceland for their generous support during the field measurements done during the Litli-Hrútur eruption. A special thanks to Kevin Cullinan and Thomas Brachmann of the University at Buffalo Instrument Machine Shop for their countless hours of work on developing the customized parts used in the penetrometer device. We are indebted to Travis Parsons for his crucial help with the logistics of assembly, transport, and use of the penetrometer throughout its creation, testing, and field use.

XI. FUNDING

Funding for the high-temperature tests at UB and fieldwork in Iceland was provided by the UB geohazards center and NSF EAR RAPID Award No. 2241489. This project also received support from NSF EAR Award No. 2223098, the Institut de Recherche pour le Développement (IRD), and the French Government Laboratory of Excellence Initiative No. ANR-10-LABX-0006. This is a Laboratory of Excellence ClerVolc Contribution No. xxx.

XII. DATA AVAILABILITY

All data that support the findings of this study are available upon the request of the corresponding author. The software is openly available at

https://github.com/LAVAPUBMH/Lava_Field_Penetrometer

XIII. REFERENCES

Alidibirov, M., and Dingwell, D.B., 1996, Magma fragmentation by rapid decompression: Nature, v. 380, p. 146–148, doi:10.1038/380146a0.

Avard, G., and Whittington, A.G., 2012, Rheology of arc dacite lavas: Experimental determination at low strain rates: Bulletin of Volcanology, v. 74, p. 1039–1056, doi:10.1007/s00445-012-0584-2.

Belousov, A., and Belousova, M., 2018, Dynamics and viscosity of ‘a’a and pahoehoe lava flows

552 of the 2012–2013 eruption of Tolbachik volcano, Kamchatka (Russia): Bulletin of
553 Volcanology, v. 80, doi:10.1007/s00445-017-1180-2.

554 Boutet, M., Dore, G., Bilodeau, J.P., and Pierre, P., 2011, Development of models for the
555 interpretation of the dynamic cone penetrometer data: International Journal of Pavement
556 Engineering, v. 12, p. 201–214, doi:10.1080/10298436.2010.488727.

557 Cashman, K. V, Soule, S.A., Mackey, B.H., Deligne, N.I., Deardorff, N.D., and Dietterich, H.R.,
558 2013, How lava flows: New insights from applications of lidar technologies to lava flow
559 studies: Geosphere, v. 9, p. 1664–1680, doi:10.1130/GES00706.1.

560 Chevrel, M.O., Cimarelli, C., DeBiasi, L., Hanson, J.B., Lavallée, Y., Arzilli, F., and Dingwell,
561 D.B., 2015, Viscosity measurements of crystallizing andesite from Tungurahua volcano
562 (Ecuador): Geochemistry Geophysics Geosystems, p. 1–20, doi:10.1002/2014GC005661.

563 Chevrel, M.O., Harris, A.J.L., James, M.R., Calabrò, L., Gurioli, L., and Pinkerton, H., 2018a,
564 The viscosity of pāhoehoe lava: In situ syn-eruptive measurements from Kilauea, Hawaii:
565 Earth and Planetary Science Letters, v. 493, p. 161–171,
566 doi:https://doi.org/10.1016/j.epsl.2018.04.028.

567 Chevrel, M.O., Labroquère, J., Harris, A.J.L., and Rowland, S.K., 2018b, PyFLOWGO: An
568 open-source platform for simulation of channelized lava thermo-rheological properties:
569 Computers and Geosciences, v. 111, p. 167–180, doi:10.1016/j.cageo.2017.11.009.

570 Chevrel, M.O., Latchimy, T., Batier, L., Delpoux, R., Harris, M.A., and Kolzenburg, S., 2023, A
571 new portable field rotational viscometer for high-temperature melts: Review of Scientific
572 Instruments, v. 94, doi:https://doi.org/10.1063/5.0160247.

573 Chevrel, M.O., Pinkerton, H., and Harris, A.J.L., 2019, Measuring the viscosity of lava in the
574 field: A review: Earth-Science Reviews, v. 196, doi:10.1016/j.earscirev.2019.04.024.

575 Dobson, K.J. et al., 2020, Quantifying Microstructural Evolution in Moving Magma: Frontiers in
576 Earth Science, v. 8, p. 1–22, doi:10.3389/feart.2020.00287.

577 Dubbelboer, A., Janssen, J.J.M., Zondervan, E., and Meuldijk, J., 2018, Steady state analysis of
578 structured liquids in a penetrometer: Journal of Food Engineering, v. 218, p. 50–60,
579 doi:10.1016/j.jfoodeng.2017.09.002.

580 Einarsson, T., 1949, Rate of Production of Material During the Eruption: The Flowing Lava:
581 Studies of Its Main Physical and Chemical Properties: Societas Scientarium Islandica, v. 4.

582 Einarsson, T., 1966, Studies of temperature, viscosity, density and some types of materials
583 produced in the Surtsey eruption: Surtsey Res Program Report, v. 1, p. 163–179.

584 Di Fiore, F., Vona, A., Kolzenburg, S., Mollo, S., and Romano, C., 2021, An Extended
585 Rheological Map of Pāhoehoe—'A'ā Transition: Journal of Geophysical Research: Solid
586 Earth, v. 126, p. 1–23, doi:10.1029/2021JB022035.

587 Floyer, J.A., and Jamieson, B.J., 2010, Rate-effect experiments on round-tipped penetrometer
588 insertion into uniform snow: Journal of Glaciology, v. 56, p. 664–672,
589 doi:10.3189/002214310793146322.

590 Fulcher, G.S., 1925, Analysis of recent measurements of the viscosity of glasses: Journal of
591 American Ceramic Society, v. 8.

592 Gauthier, F., 1973, Field and Laboratory Studies of the Rheology of Mount Etna Lava:
593 Philosophical Transactions of the Royal Society A: Mathematical, Physical and Engineering
594 Sciences, v. 274, p. 83–98.

595 Giordano, D., and Dingwell, D.B., 2003, Viscosity of hydrous Etna basalt: Implications for
596 Plinian-style basaltic eruptions: Bulletin of Volcanology, v. 65, p. 8–14,
597 doi:10.1007/s00445-002-0233-2.

598 Giordano, D., Russell, J.K., and Dingwell, D.B., 2008, Viscosity of magmatic liquids: A model:
599 Earth and Planetary Science Letters, v. 271, p. 123–134, doi:10.1016/j.epsl.2008.03.038.

600 Hall, R., Stumpf, A., Baji, A., Ross, R., and Barnett, D., 2022, Characterising Penetrometer Tip
601 Contact during Concrete Condition Assessment: Sensors, v. 22, p. 1–12,
602 doi:10.3390/s22030737.

603 Harris, C.R. et al., 2020, Array programming with NumPy: Nature, v. 585, p. 357–362,
604 doi:10.1038/s41586-020-2649-2.

605 Harris, A.J.., and Allen, J.S., 2008, One-, two- and three-phase viscosity treatments for basaltic
606 lava flows: Journal of Geophysical Research, v. 113, doi:10.1029/2007JB005035.

607 Harris, A.J.L., and Rowland, S.K., 2015, Lava Flows and Rheology: Elsevier Inc., 321–342 p.,
608 doi:10.1016/b978-0-12-385938-9.00017-1.

609 Heap, M.J., Xu, T., and Chen, C., 2014, The influence of porosity and vesicle size on the brittle
610 strength of volcanic rocks and magma: Bulletin of Volcanology, v. 76, p. 1–15,
611 doi:10.1007/s00445-014-0856-0.

612 Herrick, J.E., and Jones, T.L., 2002, A dynamic cone penetrometer for measuring soil
613 penetration resistance: Soil Science Society of America Journal, v. 66, p. 1320–1324,
614 doi:10.2136/sssaj2002.1320.

615 Hess, K.U., Cordonnier, B., Lavalĺe, Y., and Dingwell, D.B., 2007, High-load, high-temperature
616 deformation apparatus for synthetic and natural silicate melts: Review of Scientific
617 Instruments, v. 78, doi:10.1063/1.2751398.

618 Hess, K.U., and Dingwell, D.B., 1996, Viscosities of hydrous leucogranitic melts: a non-
619 Arrhenian model: American Mineralogist, v. 81, p. 1297–1300.

620 Hobiger, M., Sonder, I., Büttner, R., and Zimanowski, B., 2011, Viscosity characteristics of
621 selected volcanic rock melts: Journal of Volcanology and Geothermal Research, v. 200, p.
622 27–34, doi:10.1016/j.jvolgeores.2010.11.020.

623 Hon, K., Gansecki, C., and Kauahikaua, J., 2003, The transition from ’A’ā to pāhoehoe crust on
624 flows emplaced during the Pu’u ’Ō’ō-Kūpaianaha eruption: US Geological Survey
625 Professional Paper, p. 89–103.

626 Huang, Z., and Aode, H., 2009, A laboratory study of rheological properties of mudflows in
627 Hangzhou Bay, China: International Journal of Sediment Research, v. 24, p. 410–424,
628 doi:10.1016/S1001-6279(10)60014-5.

629 Hunter, J.D., 2007, Matplotlib: A 2D Graphics Environment: Computing in Science and
630 Engineering, v. 9, p. 90–95, doi:10.1109/MCSE.2007.55.

631 Jantra, C., Slaughter, D.C., Roach, J., and Pathaveerat, S., 2018, Development of a handheld
632 precision penetrometer system for fruit firmness measurement: Postharvest Biology and
633 Technology, v. 144, p. 1–8, doi:https://doi.org/10.1016/j.postharvbio.2018.05.009.

Kauahikaua, J., Sherrod, D.R., Cashman, K. V., Heliker, C., Hon, K., Mattox, T.N., and Johnson, J.A., 2003, Hawaiian lava-flow dynamics during the Pu'u 'Ō'ō-Kū paianaha eruption: A tale of two decades: US Geological Survey Professional Paper, p. 63–87.

Keszthelyi, L.P., 1994, On the Thermal Budget of Pahoehoe Lava Flows: California Institute of Technology, 274 p.

Kirkham, M.B., 2014, Chapter 11 - Penetrometers, *in* Kirkham, M.B.B.T.-P. of S. and P.W.R. (Second E. ed., Principles of Soil and Plant Water Relations, Boston, Academic Press, p. 171–183, doi:https://doi.org/10.1016/B978-0-12-420022-7.00011-2.

Kolzenburg, S., Chevrel, M.O., and Dingwell, D.B., 2022, Magma / Suspension Rheology: Reviews in Mineralogy and Geochemistry, v. 87, p. 639–720, doi:10.2138/rmg.2022.87.14.

Kolzenburg, S., Giordano, D., Di Muro, A., and Dingwell, D.B., 2019, Equilibrium viscosity and disequilibrium rheology of a high magnesium basalt from piton de la fournaise volcano, la reunion, indian ocean, France: Annals of Geophysics, v. 62, doi:10.4401/ag-7839.

Kolzenburg, S., Hess, K.-U., Berlo, K., and Dingwell, D.B., 2020, Disequilibrium Rheology and Crystallization Kinetics of Basalts and Implications for the Phlegrean Volcanic District: Frontiers in Earth Science, v. 8, doi:10.3389/feart.2020.00187.

Kostynick, R., Matinpour, H., Pradeep, S., Haber, S., Sauret, A., Meiburg, E., Dunne, T., Arratia, P., and Jerolmack, D., 2022, Rheology of debris flow materials is controlled by the distance from jamming: Proceedings of the National Academy of Sciences of the United States of America, v. 119, p. 1–10, doi:10.1073/pnas.2209109119.

Llewellin, E.W., Mader, H.M., and Wilson, S.D.R., 2002, The constitutive equation and flow dynamics of bubbly magmas: Geophysical Research Letters, v. 29, p. 1–4, doi:10.1029/2002GL015697.

Macosko, C.W., 1994, Rheology: Principles, Measurements and Applications, p. 1–576, https://app.knovel.com/hotlink/pdf/id:kt0059EKWM/rheology-principles-measurements/part-i-constitutive-relations.

Mader, H.M., Llewellin, E.W., and Mueller, S.P., 2013, The rheology of two-phase magmas: A review and analysis: Journal of Volcanology and Geothermal Research, v. 257, p. 135–158,

doi:10.1016/j.jvolgeores.2013.02.014.

Marsh, B.D., 1981, On the crystallinity, probability of occurrence, and rheology of lava and magma: Contributions to Mineralogy and Petrology, v. 78, p. 85–98, doi:10.1007/BF00371146.

Moitra, P., and Gonnermann, H.M., 2015, Effects of crystal shape- and size-modality on magma rheology: Geochemistry, Geophysics, Geosystems, v. 16, p. 1–26, doi:10.1002/2014GC005554.

De Moraes, M.T., Da Silva, V.R., Zwirtes, A.L., and Carlesso, R., 2014, Use of penetrometers in agriculture: A review: Engenharia Agricola, v. 34, p. 179–193, doi:10.1590/S0100-69162014000100019.

Panov, V.K, Slezin, Yu. B, and Storcheus, A.V, 1988, Mechanical Properties of Lava Extruded in 1983 Predskazannyi Eruption (Klyuchevskoi Volcano): Journal of Volcanol Seismol, v. 7, p. 25–37.

Pinkerton, H., 1978, Methods of measuring the rheological properties of lava.: Ph.D. Lancaster.

Pinkerton, H., Herd, R.A., Kent, R.M., and Wilson, L., 1995a, Field Measurements of the Rheological Properties of Basaltic Lavas, *in* Abstracts of the Lunar and Planetary Science Conference, p. 1127–1128.

Pinkerton, H., and Norton, G., 1995, Rheological properties of basaltic lavas at sub-liquidus temperatures: laboratory and field measurements on lavas from Mount Etna: Journal of Volcanology and Geothermal Research, v. 68, p. 307–323, doi:10.1016/0377-0273(95)00018-7.

Pinkerton, H., Norton, G.E., Dawson, J.B., and Pyle, D.M., 1995b, Field Observations and Measurements of the Physical Properties of Oldoinyo Lengai Alkali Carbonatite Lavas, November 1988 BT - Carbonatite Volcanism: Oldoinyo Lengai and the Petrogenesis of Natrocarbonatites, *in* Bell, K. and Keller, J. eds., Berlin, Heidelberg, Springer Berlin Heidelberg, p. 23–36, doi:10.1007/978-3-642-79182-6_3.

Pinkerton, H., and Sparks, R.S.J., 1978, Field measurements of the rheology of lava: Nature, v. 276, p. 383–385, doi:10.1038/276383a0.

690 Pinkerton, H., and Stevenson, R.J., 1992, Methods of determining the rheological properties of
691 magmas at sub-liquidus temperatures: Journal of Volcanology and Geothermal Research, v.
692 53, p. 47–66, doi:10.1016/0377-0273(92)90073-M.

693 Pistone, M., Caricchi, L., Ulmer, P., Reusser, E., and Ardia, P., 2013, Rheology of volatile-
694 bearing crystal mushes: Mobilization vs. viscous death: Chemical Geology, v. 345, p. 16–
695 39, doi:10.1016/j.chemgeo.2013.02.007.

696 Robert, B., Harris, A., Gurioli, L., Médard, E., Sehlke, A., and Whittington, A., 2014, Textural
697 and rheological evolution of basalt flowing down a lava channel: Bulletin of Volcanology,
698 v. 76, p. 1–21, doi:10.1007/s00445-014-0824-8.

699 Rognon, P.G., Chevoir, F., Bellot, H., Ousset, F., Naaïm, M., and Coussot, P., 2008, Rheology of
700 dense snow flows: Inferences from steady state chute-flow experiments: Journal of
701 Rheology, v. 52, p. 729–748, doi:10.1122/1.2897609.

702 Rust, A.C., and Manga, M., 2002, Effects of bubble deformation on the viscosity of dilute
703 suspensions: Journal of Non-Newtonian Fluid Mechanics, v. 104, p. 53–63,
704 doi:10.1016/S0377-0257(02)00013-7.

705 Sato, H., 2005, Viscosity measurement of subliquidus magmas: 1707 basalt of Fuji volcano:
706 Journal of Mineralogical and Petrological Sciences, v. 100, p. 133–142,
707 doi:10.2465/jmps.100.133.

708 Schneebeli, M., and Johnson, J.B., 1998, A constant-speed penetrometer for high-resolution
709 snow stratigraphy: Annals of Glaciology, v. 26, p. 1–5,
710 doi:https://doi.org/10.3189/1998AoG26-1-107-111.

711 Sehlke, A., Whittington, A., Robert, B., Harris, A., Gurioli, L., and Médard, E., 2014, Pahoehoe
712 to áá transition of Hawaiian lavas: An experimental study: Bulletin of Volcanology, v. 76,
713 doi:10.1007/s00445-014-0876-9.

714 Shaw, H.R., 1969, Rheology of basalt in the melting range: Journal of Petrology, v. 10, p. 510–
715 535, doi:10.1093/petrology/10.3.510.

716 Shaw, H.R., Wright, T.L., Peck, D.L., and Okamura, R., 1968, The Viscosity of Basaltic Magma:
717 An Analysis of Field Measurements in Makaopuhi Lava Lake, Hawaii: American Journal of

718 Science, v. 266, p. 225–264.

719 Tanaka, M., De Man, J.M., and Voisey, P.W., 1971, Measurement of textural properties of foods
720 with a constant speed cone penetrometer: Journal of Texture Studies, v. 2, p. 306–315,
721 doi:https://doi.org/10.1111/j.1745-4603.1971.tb01007.x.

722 Tanaka, M., Pearson, A.M., and deMan, J.M., 1972, Measurement of Ice Cream Texture with the
723 Constant Speed Penetrometer: Canadian Institute of Food Science and Technology Journal,
724 v. 5, p. 105–110, doi:https://doi.org/10.1016/S0315-5463(72)74098-5.

725 Truby, J.M., Mueller, S.P., Llewellin, E.W., and Mader, H.M., 2015, The rheology of three-
726 phase suspensions at low bubble capillary number: Proceedings of the Royal Society A:
727 Mathematical, Physical and Engineering Sciences, v. 471, doi:10.1098/rspa.2014.0557.

728 Vogel, D.H., 1921, Temperaturabhängigkeitsgesetz der Viskosität von Flüssigkeiten:
729 Physikalische Zeitschrift, v. 22, p. 645.

730 Widjaja, B., 2019, Landslide and Mudflow Behavior Case Study in Indonesia: Rheology
731 Approach: IPTEK Journal of Proceedings Series, v. 0, p. 93,
732 doi:10.12962/j23546026.y2019i3.5849.

Post-print version of the article published in Review in Scientific Instrument. Vol. 95, 065103 (2024) https://doi.org/10.1063/5.0206776

XIV. FIGURES

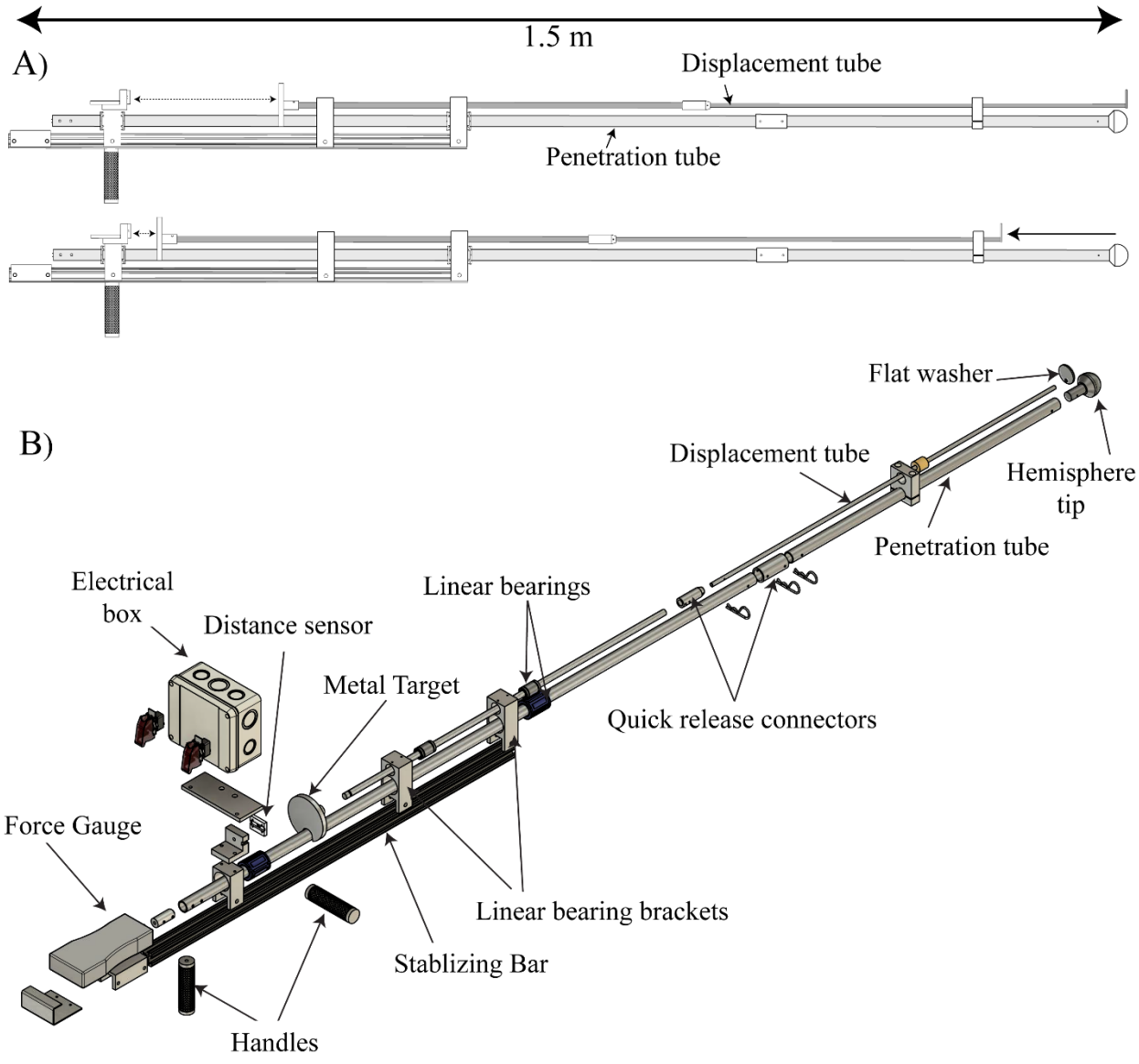

Figure 1: Computer-aided design (CAD) rendering of the new penetrometer device for rheology measurements. A) Simple profile views that highlight the two main components, 1) the penetration tube and 2) the displacement tube, with the relative motion of the displacement tube shown. B) An exploded view of the major components of the penetrometer. Drawings of all individual custom machined parts with detailed specifications can be found within

supplementary material 1. CAD image rendering done by Thomas Brachmann (UB CAS machine shop technician), at a scale of 1:7.

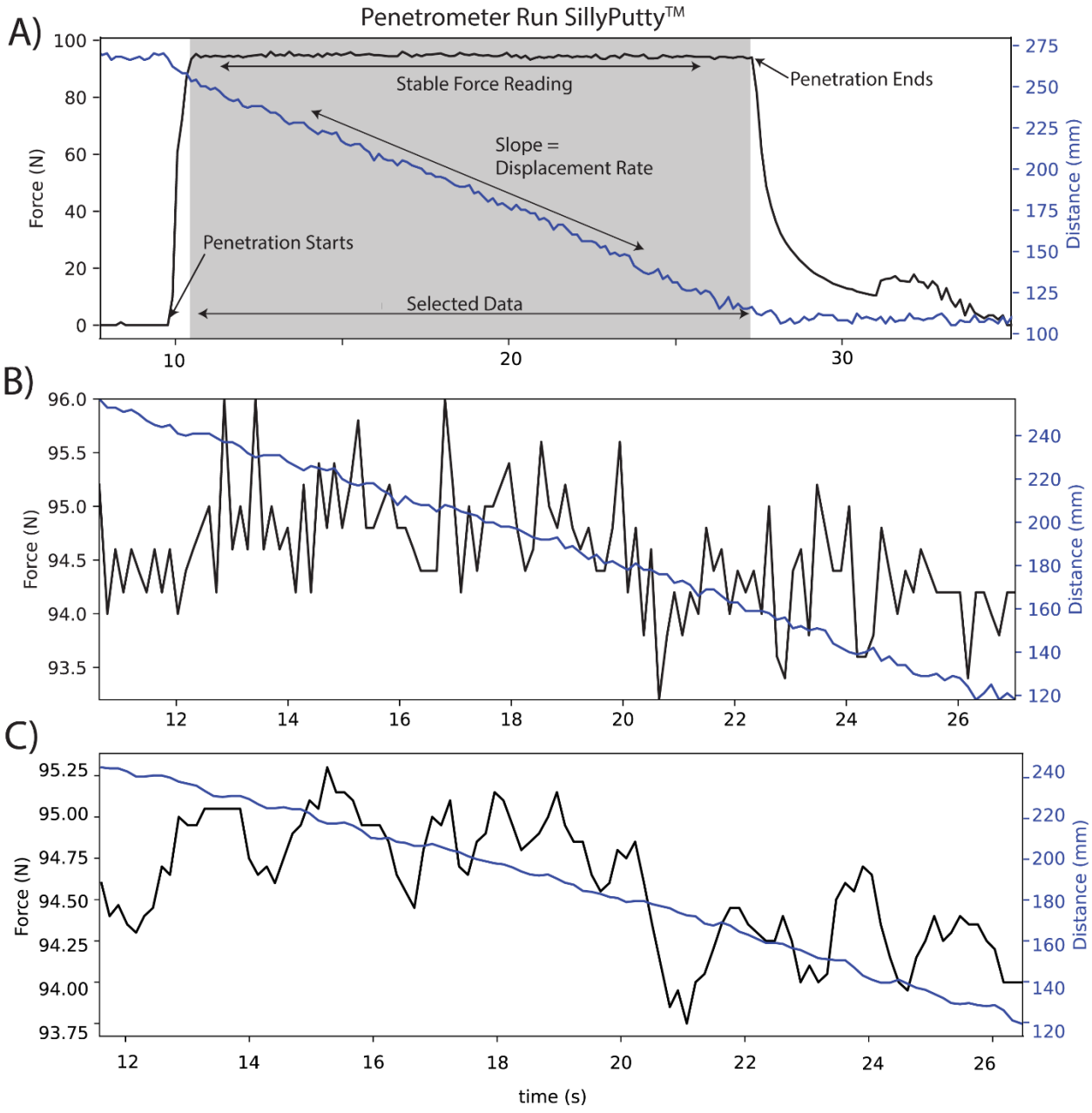

Figure 2: Examples of data recorded from penetrometer during testing with SillyPutty™. A) Full record of raw data from the output text file, with time on the x-axis, Force (N) on the y-axis (left), and displacement (mm) on the y-axis (right). The data recorded by the force gauge is shown in black and data recorded by the distance sensor is shown in blue. The grey field is the area of data selection shown in B. B) Extracted raw data from the selected portion (grey) in

subplot A. C) The data shown here is processed after a moving average function (window of five) that smooths some of the sensor noise. This data is then used to calculate the changing force with displacement (velocity) throughout the measurement. These values of force and velocity are used to calculate the viscosity of the measured material (here SillyPutty^{TM}).

Post-print version of the article published in Review in Scientific Instrument. Vol. 95, 065103 (2024) https://doi.org/10.1063/5.0206776

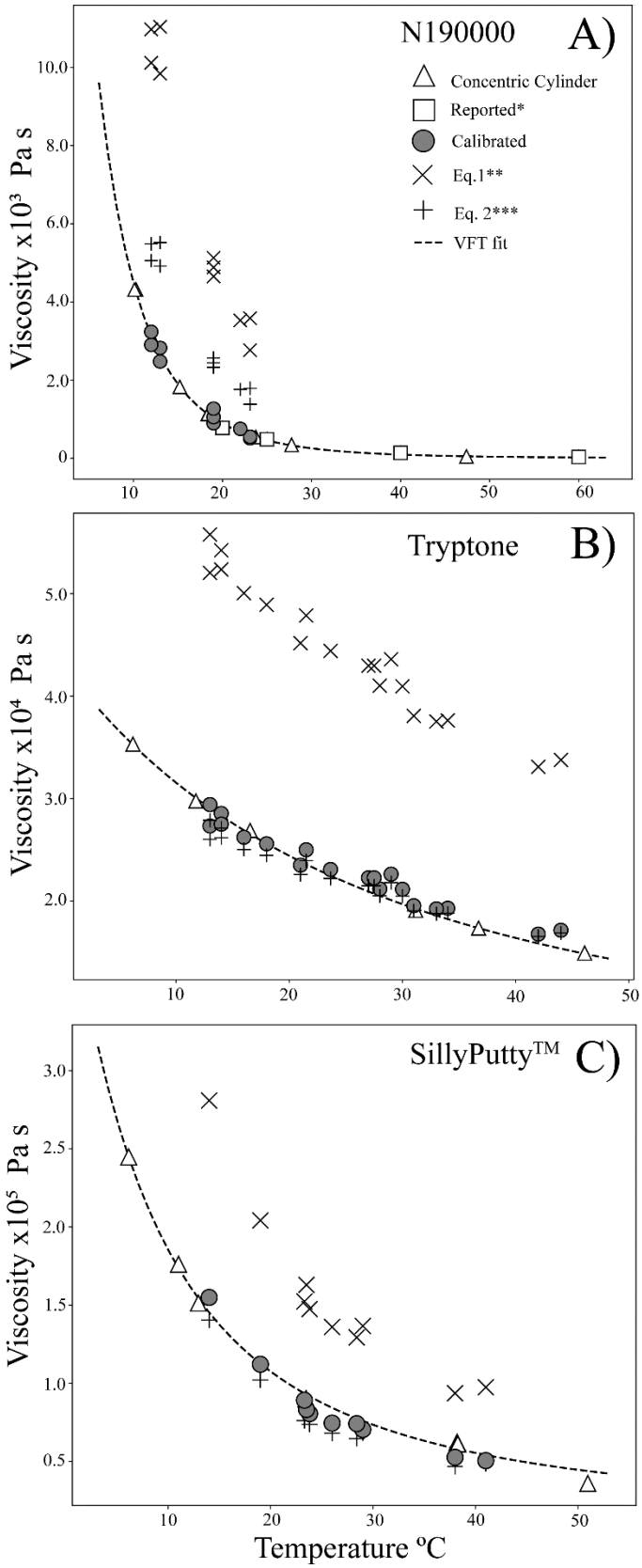

Figure 3: Plots showing the temperature-dependent viscosity of N190000 (A), Tryptone (B), and SillyPutty™ (C). The data measured with a concentric cylinder rheometer is shown with triangles and a VFT fit to the data as a dashed line. The values recovered from the penetrometer data following the calibration procedure detailed in the text are shown with grey circle symbols. * certified viscosity values for N190000 as given by Cannon®, shown as squares. **Viscosities derived from modified Stoke's Law (Eq.1) are shown as cross symbols. ***Viscosities derived from Stoke's Law (Eq.2) are shown as plus symbols. Individual points are larger than the uncertainty.

Post-print version of the article published in Review in Scientific Instrument. Vol. 95, 065103 (2024) https://doi.org/10.1063/5.0206776

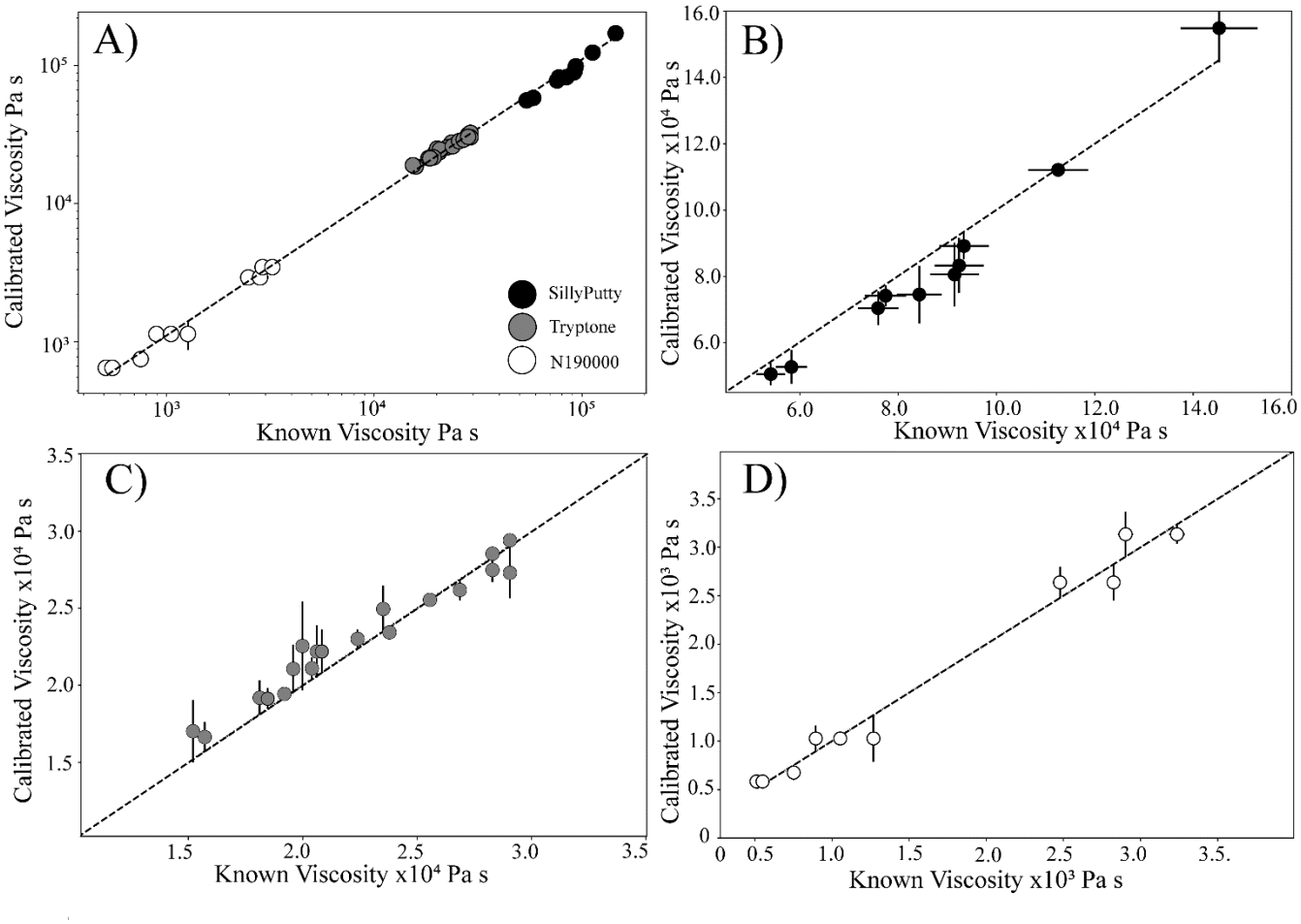

Figure 4: Plots showing measured viscosity values with the new penetrometer versus the known viscosity of the material for three different analog materials. Here the measured values are derived from the penetrometer sensor data with the calibration factors applied. The known values are from NIST traceable standards and traceable internal reference materials. A) The full range of three analog materials. B) SillyPutty™. C) Tryptone. D)N190000 Oil. The dashed line gives the 1:1 relationship. Error bars are 2σ.

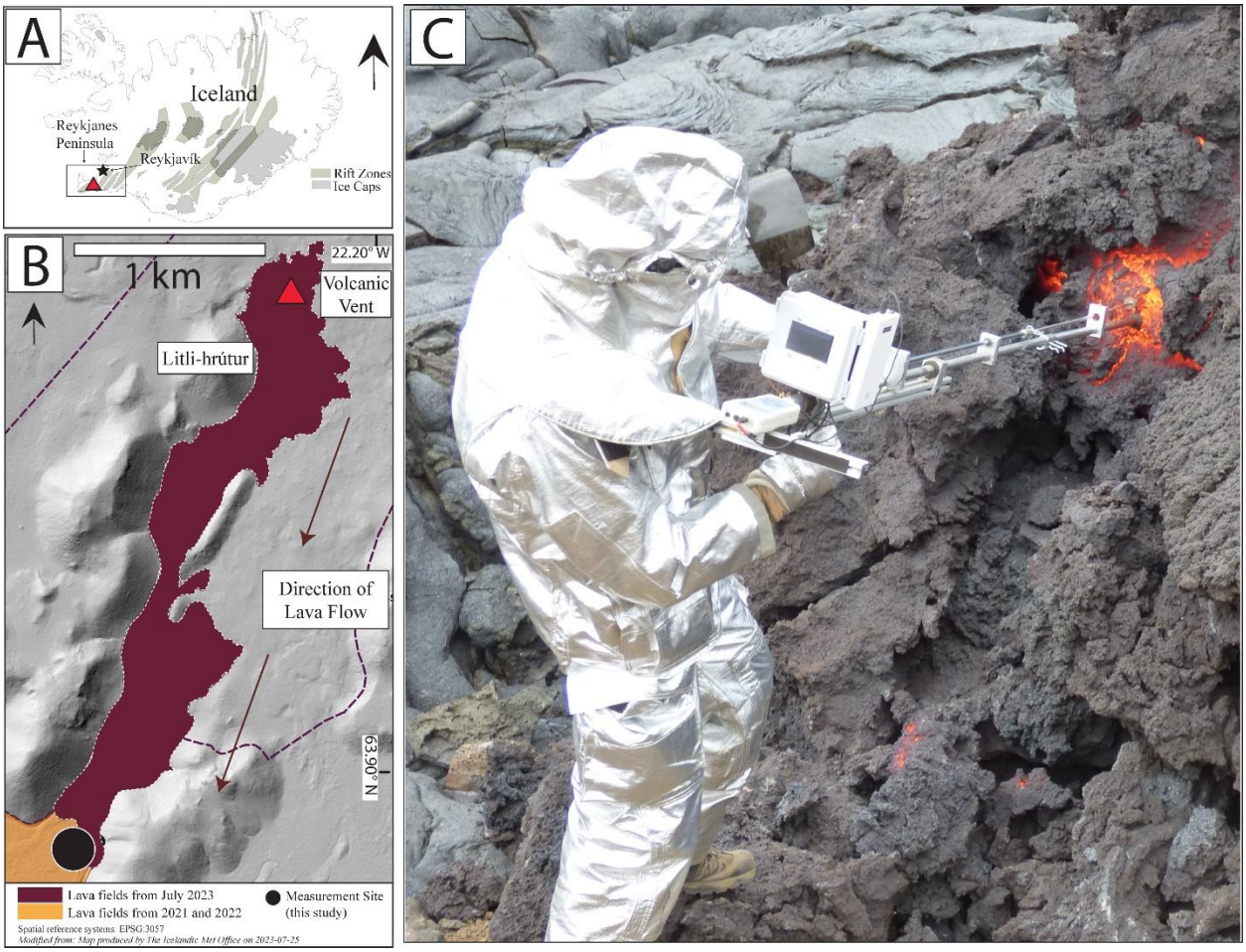

Figure 5: Map of 2023 Litli-Hrútur Eruption in Iceland and view of field usage of the penetrometer. The black vertical arrows denote North. A) Regional setting of the eruption within the southwest Reykjanes Peninsula. The red triangle denotes the vent location. Rift zones and ice caps are shown in dark and light grey, respectively. B) Map showing the extent of the lava flow field from the Litli-Hrútur eruption on July 25, 2023. C) Field usage of the penetrometer, the operator is 1.88 meters tall for scale.

Post-print version of the article published in Review in Scientific Instrument. Vol. 95, 065103 (2024) https://doi.org/10.1063/5.0206776

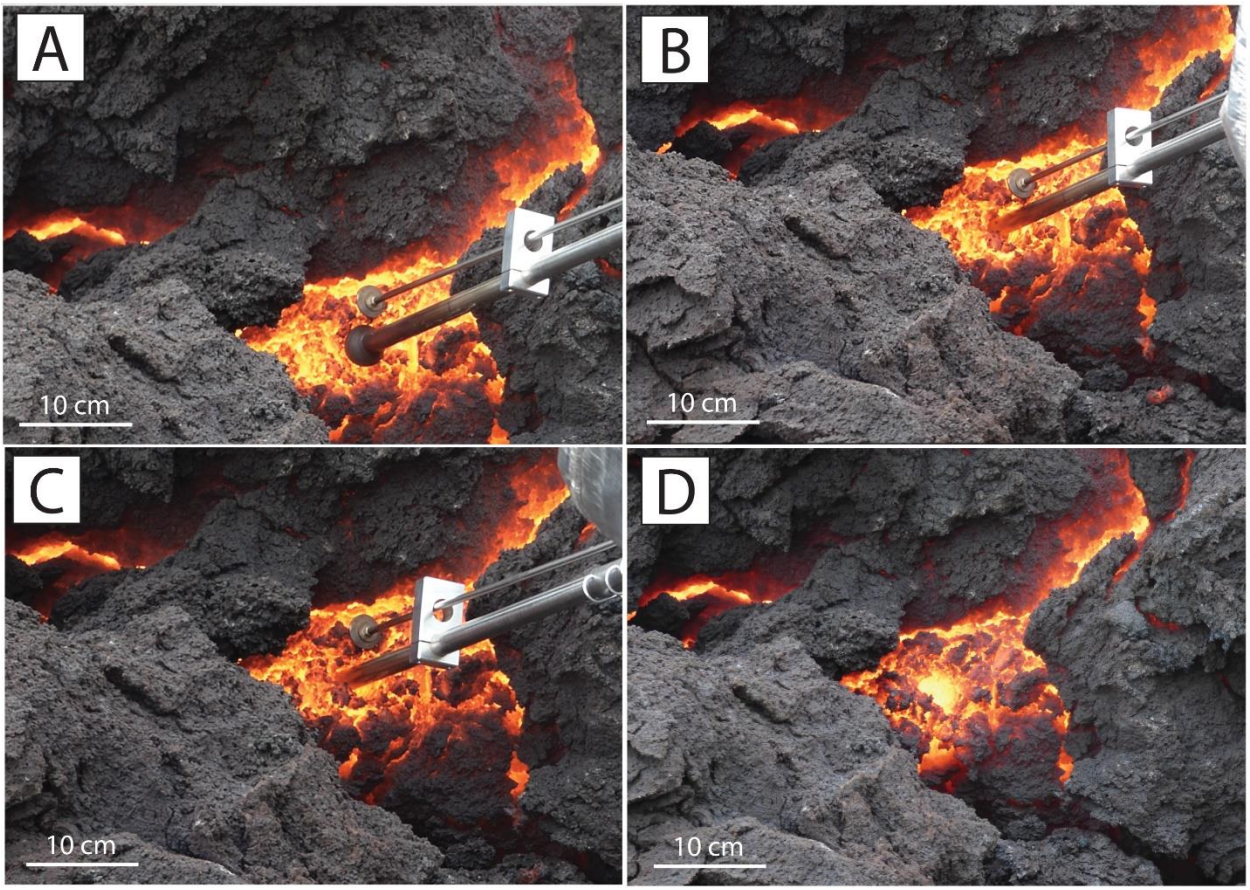

Figure 6: A close view of the progression of the lava penetrometer used in high-temperature lava. A-C) shows the progression of the hemisphere entering the lava while the displacement rod rests on the exterior crust. D) Shows the hole left in the lava after penetrometer extraction with a diameter of the penetrometer tip.

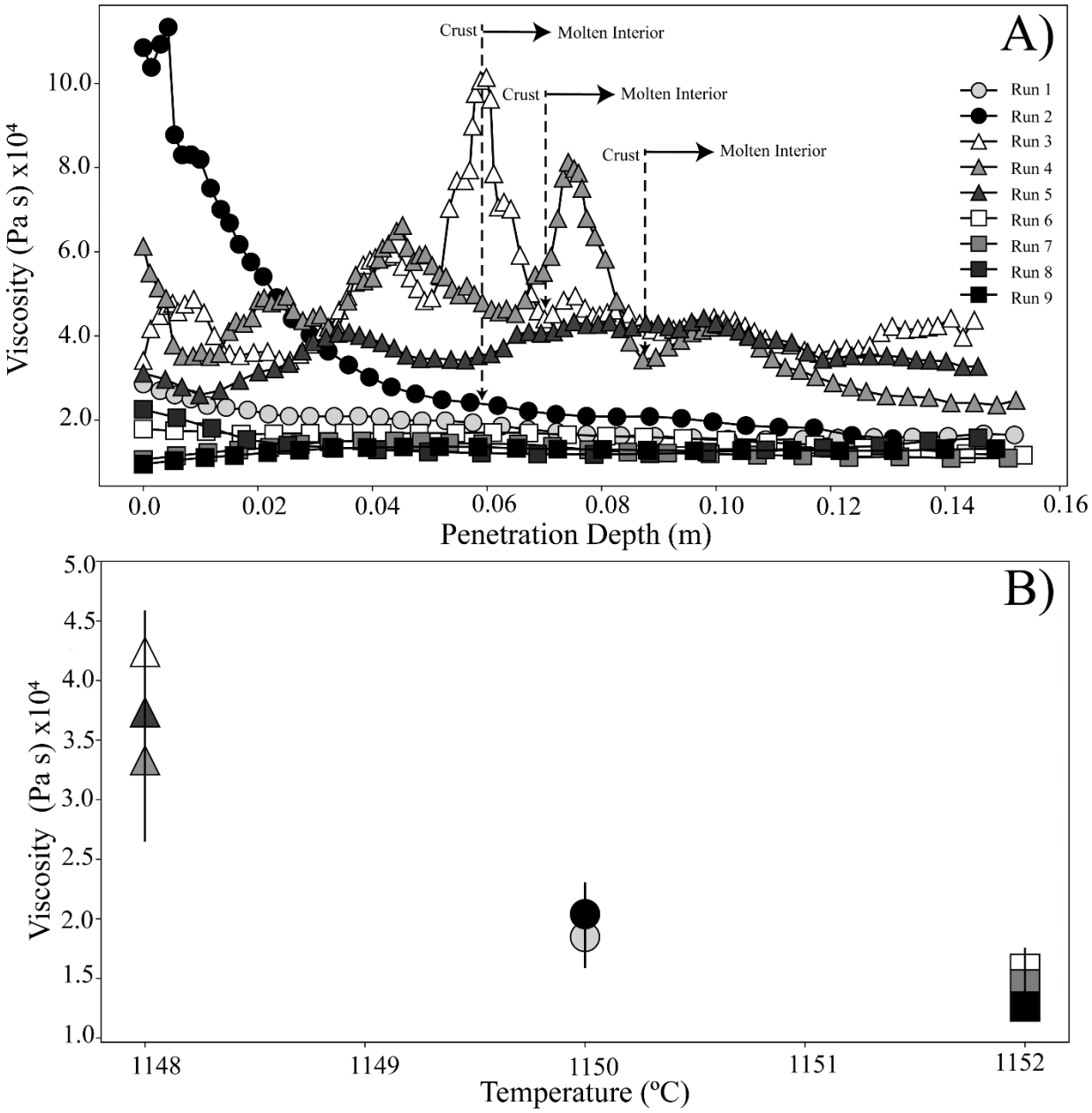

Figure 7: Plots showing the processed data from nine penetrometer measurements within lava from the Litli-Hrútur eruption at the single location shown in Figure 5. A) Measured viscosity (Pa s) versus the depth of penetration (m). The dashed line with arrow symbols indicates runs where initially high or fluctuating viscosity values are followed by a decrease and then stabilized viscosity. Data on the left of the arrow are interpreted as crustal penetration and the right of the arrow is interpreted as the molten interior. The changing viscosity profiles for Runs 2-4 display the penetrometer's ability to capture transient rheological properties of a heterogeneous material within a single measurement. B) The viscosity (Pa s) of only the molten interior plotted against the temperature (˚C) of the molten interior. The data document the temperature-dependent viscosities with nearly a three-fold increase in apparent viscosity within a temperature decrease

of 4˚C. The temperatures were recovered from the same K-type thermocouple (±1˚C) inserted into the lava adjacent to the measurement sites.